Real-time Navigation for Mars Final Approach Using X-ray Pulsars

Conference Paper · August 2013

DOI: 10.2514/6.2013-5204

4 authors, including:

Zheng-shi Yu
Beijing Institute of Technology
32 PUBLICATIONS **363** CITATIONS

SEE PROFILE

AIAA 2013-5204

Real-time Navigation for Mars Final Approach Using X-ray Pulsars

Pingyuan Cui*, Zhengshi Yu†, Shengying Zhu‡, and Ai Gao§
School of Aerospace Engineering, Beijing Institute of Technology, Beijing, People's Republic of China, 100081

Key Laboratory of Dynamics and Control of Flight Vehicle, Ministry of Education, Beijing, People's Republic of China, 100081

An accurate knowledge of Mars entry condition is the significant requirement for the successful aerocapture and pinpoint landing. In order to develop the real-time navigation scheme for Mars final approach, the feasibility of navigation embedded X-ray pulsar observations is verified, and the navigation performance is comparatively analyzed. In order to choose optimal navigation pulsars from pulsar candidates, the Fisher information matrix is utilized to evaluate the observability from the estimation theory point of view. The optimal navigation pulsars thus are selected such that the determinant of the Fisher information matrix is maximal. Two navigation scenarios based on the 2012 encounter at Mars of Curiosity spacecraft combining with X-ray pulsar based measurements are then considered to demonstrate the navigation performance. Furthermore, a series of research on the error ellipse in Mars B-plane and the distribution of estimated flight path angle indicate that X-ray pulsar based navigation, which may provide more accurate knowledge of Mars entry condition, is a potential navigation scheme for Mars final approach in the future.

Nomenclature

c	=	speed of light
f_T	=	transmitted signal frequency
$\boldsymbol{F}$	=	Fisher information matrix
$\boldsymbol{h}$	=	nonlinear measurement operator
$\boldsymbol{K}$	=	Kalman gain matrix of state mean
$\tilde{\boldsymbol{K}}$	=	Kalman gain matrix of state deviations
$\boldsymbol{n}$	=	direction vector of X-ray pulsar
N	=	size of ensemble elements
$\boldsymbol{r}_s$	=	position vector of spacecraft
R	=	radial range between the spacecraft and orbiter
$\dot{R}$	=	the radial velocity between the spacecraft and orbiter
$\boldsymbol{v}_s$	=	velocity vector of spacecraft
$\boldsymbol{X}$	=	state vector of navigation filter
$\boldsymbol{y}$	=	observation vector
μ	=	gravitational parameter
Δf	=	Doppler shift
Δt	=	time difference between the time-of-arrival at spacecraft and solar system barycenter

* Corresponding author, Professor, Mail box 22, School of Aerospace Engineering, Beijing institute of Technology, Haidian District, Beijing, cuipy@bit.edu.cn.
† Ph.D. Candidate, Mail box 22, School of Aerospace Engineering, Beijing institute of Technology, Haidian District, Beijing, yuzhengshi@gmail.com.
‡ Lecturer, Mail box 22, School of Aerospace Engineering, Beijing institute of Technology, Haidian District, Beijing, zhushengying@gmail.com.
§ Lecturer, Mail box 22, School of Aerospace Engineering, Beijing institute of Technology, Haidian District, Beijing, gaoai@bit.edu.cn.

I. Introduction

PRECISION landing at predefined location of the great scientific interests may be required in order to achieve valuable scientific goals for the next generation of Mars exploration. The NASA's Mars Technology Program has identified pinpoint landing as a key advanced technology for future Mars exploration[1]. The latest Mars exploration mission of Curiosity has taken a major step toward precision landing on Mars[2]. Employing guided entry with banking maneuvers, this spacecraft set down within 2 km of the landing target. The knowledge of entry condition, especially flight path angle (FPA), may have significant impact on the accuracy of aerocapture and pinpoint landing. Therefore, real-time navigation during the final approach phase of Mars landing mission is the main contributor to fulfilling the requirement for future Mars exploration.

The radio antennas of NASA's Deep Space Network (DSN), which are located in Goldstone (California), Madrid (Spain), and Canberra (Australia), together with the radio system mounted on the spacecraft, are primarily utilized to provide navigation measurements for Mars exploration[3]. The traditional measurements of radiometric Doppler and range are used by Mars exploration missions in most mission phases to determine the spacecraft radial velocity and range[4,5]. Furthermore, in order to improve navigation performance by determining the spacecraft angular position, ΔDOR measurements are employed in conjunction with Doppler and range data[6]. The Curiosity mission used these three types of tracking information from DSN as assessments of the spacecraft's trajectory. Navigation during the cruise and initial approach phase is mostly relying on the ground based Earth observation because there is sufficient time to relay telemetry and uplink commands to the spacecraft. However, the final approach phases are short and the navigation must be performed without ground based Earth support because of severe time delay. So the trajectory knowledge updates after the ground based data cutoff, which is typically 6h before entry, must be obtained in situ and processed onboard.

The Mars Network, which consists of radio beacons such as Mars orbiter and ground based beacons, is ideally located to provide spacecraft-to-spacecraft or spacecraft-to-beacon radiometric navigation data. Using the Electra ultrahigh frequency (UHF) transceiver, relative radial velocity and range can be provided by measuring the Doppler and range signals. Therefore the navigation can be processed onboard in real time during the final approach and EDL phases[7,8]. To resolve the observability issue during the Mars entry phase, Lévesque[9] proposed innovative measurement scenarios based on radio range provided from reference radio beacons with known positions. Pastor[10] quantified the benefits to Mars entry navigation using Doppler and range observations, and analyzed the navigation accuracy of different beacon configurations. Ely[11] examined the performance of the Mars Network of providing approach navigation services given tracking capabilities, and showed that Mars Network Doppler is a robust data type which can improve trajectory knowledge accuracy. Lightsey[12] conducted a set of analyses based on the Curiosity mission combining with the Mars Reconnaissance Orbiter (MRO), and demonstrated that the navigation system could achieve a 300m entry knowledge error. However, because of the occlusion of Mars, the line of sight visibility between the spacecraft and orbiter dose not exist all the time. Therefore, additional measurements should be brought in during these invisible periods to achieve the real-time navigation throughout the final approach phase.

In recent years, NASA has been considering the probability of using X-ray pulsars as potential source for spacecraft navigation[13,14]. X-ray pulsars are highly magnetized and rotating neutron stars that emit X-ray signals. They provide stable, predictable, and unique signatures, which give a new answer to planetary navigation. The navigation system utilizing X-ray pulsars are available anywhere where cosmic X-ray sources can be observed. Furthermore, the system can operate in an autonomous mode, independent of DSN systems[15]. In previous investigations, Sheikh[16,17] explored the possibility of autonomous navigation using X-ray pulsars and developed the time transformation equation. Emadzadeh[18] proposed a new algorithm for relative navigation between two spacecrafts using X-ray pulsar measurements and addressed the delay estimation problem. In addition, NASA has started XNAV program to demonstrate the feasibility of X-ray pulsars based navigation and has developed relative payload and software[19]. Based on the benefits of autonomy and accuracy, navigation using X-ray pulsars may be a supplementary of real-time navigation for Mars final approach.

This paper aims to demonstrating the feasibility of embedded X-ray pulsars observations into the navigation system for Mars final approach to achieve real-time, autonomy and accuracy. In Section II, basic principles of Mars Network based navigation and X-ray pulsar based navigation are briefly investigated. Additionally, the optimal navigation pulsars are selected with the help of Fisher information matrix (FIM). Then, based on the Curiosity mission in 2012, two navigation scenarios for Mars approach in conjunction with measurements from DSN, Mars orbiter and X-ray pulsar are considered in Section III. In order to allow for the nonlinear dynamical model and observation model, ensemble squire root Kalman filter (EnSRF) is adapted. The description of filter algorithm is shown in Section IV. A series of simulations are conducted in Section V to show the benefits of X-ray pulsar based navigation. Simulation results demonstrate that X-ray pulsar based navigation can improve the performance of

navigation for Mars final approach. The autonomy and accuracy of X-ray pulsar based navigation makes it a promising navigation method for future Mars exploration. Finally, conclusions are drawn in Section VI.

II. Concept of Operation

A. Mars Network based Navigation

The Electra transceiver can provide spacecraft-to-spacecraft radiometric navigation data between a Mars approach spacecraft and a Mars Network orbiter by measuring the range and Doppler shifted signals. The Schematic of spacecraft-to-spacecraft navigation used for Mars final approach can be found in Fig. 1.

In the schematic, the position and velocity of spacecraft and orbiter are defined in heliocentric ecliptic coordinate system (J2000). We call $\boldsymbol{r}_s$ the position vector of spacecraft and $\boldsymbol{r}_m$ the position vector of Mars Network orbiter. $\boldsymbol{v}_s$ and $\boldsymbol{v}_m$ refer to the velocity vector of spacecraft and Mars Network orbiter respectively. The model of radial range of R is determined as

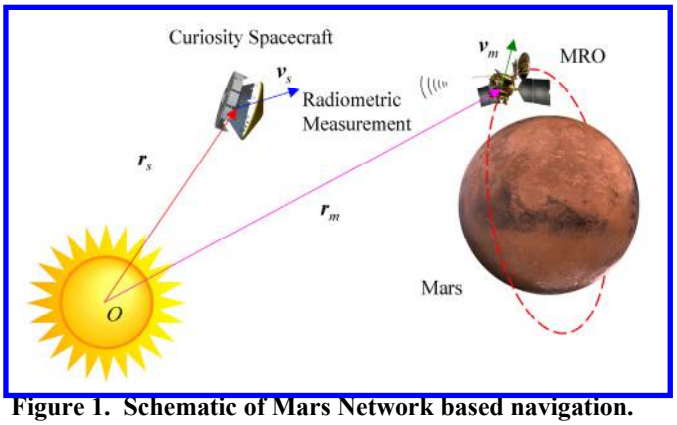

Figure 1. Schematic of Mars Network based navigation.

$$R = \left| \boldsymbol{r}_s - \boldsymbol{r}_m \right| \tag{1}$$

By measuring Doppler shifted signals the Electra transceiver may compute the radial velocity between spacecraft and orbiter. A simplified model of the Doppler shift observation is given by

$$\Delta f = -f_T \dot{R} / c \tag{2}$$

where f_T is the transmitted signal frequency, $\dot{R}$ is the radial velocity between the spacecraft and orbiter, and c is the speed of light. Since the radial velocity is given by

$$\dot{R} = \left[\left(\boldsymbol{v}_s - \boldsymbol{v}_m \right) \cdot \left(\boldsymbol{r}_s - \boldsymbol{r}_m \right) \right] / \left| \boldsymbol{r}_s - \boldsymbol{r}_m \right| \tag{3}$$

the measurement model of Doppler shift can be represented as

$$\Delta f = -f_T \left[\left(\boldsymbol{v}_s - \boldsymbol{v}_m \right) \cdot \left(\boldsymbol{r}_s - \boldsymbol{r}_m \right) \right] / \left(c \left| \boldsymbol{r}_s - \boldsymbol{r}_m \right| \right) \tag{4}$$

B. X-ray Pulsar based Navigation

In the implementation of X-ray pulsar based navigation, the X-ray sensor on a spacecraft detects the photons emitted from the pulsars to determine the arrival time of X-ray pulses. With the time-of-arrival (TOA) estimate and models of pulsar timing, the ranges of spacecraft along the unit vectors from solar system barycenter (SSB) to the pulsars can be calculated. The orbit determination can be processed with these range measurements through a navigation filter[16,17,19]. The concept of X-ray pulsar based navigation is illustrated in Fig. 2.

For X-ray pulsar based navigation, the basic measurement is the time difference between the TOA at spacecraft t_s and the TOA at SSB origin t_b which can be predicted from the model of pulsar timing. The measurement model of time difference can be constructed as

$$\begin{aligned} \Delta t = t_b - t_s = \boldsymbol{n} \cdot \boldsymbol{r}_b / c + \left[\left(\boldsymbol{n} \cdot \boldsymbol{r}_b \right)^2 - r_b^2 + 2 \left(\boldsymbol{n} \cdot \boldsymbol{b} \right) \left(\boldsymbol{n} \cdot \boldsymbol{r}_b \right) - 2 \left(\boldsymbol{b} \cdot \boldsymbol{r}_b \right) \right] / \left(2 c D_0 \right) + \\ 2 \mu_s \ln \left| \left(\boldsymbol{n} \cdot \boldsymbol{r}_b + r_b \right) / \left(\boldsymbol{n} \cdot \boldsymbol{b} + b \right) + 1 \right| / c^3 \end{aligned} \tag{5}$$

In the equation, $\boldsymbol{n}$ is the unit direction from the SSB to pulsar, $\boldsymbol{b}$ is the position of SSB relative to the sun's center, and $\boldsymbol{r}_b$ is the position of the spacecraft relative to the SSB, such that

$$\boldsymbol{r}_s = \boldsymbol{b} + \boldsymbol{r}_b \tag{6}$$

Meanwhile, b and r_b refers to the norm of $\boldsymbol{b}$ and $\boldsymbol{r}_b$ respectively. Furthermore, D_0 is called the norm of position vector of the pulsar in heliocentric ecliptic coordinate system and μ_s is called the sun's gravitational parameter. The unit direction of the pulsar can be considered constant in the solar system because most pulsars are so far away from the Sun.

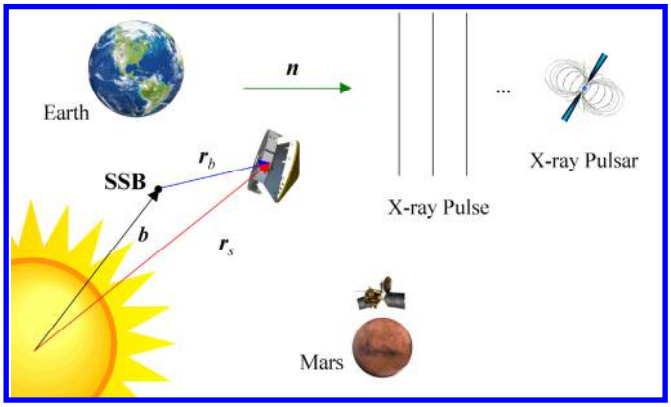

Figure 2. X-ray pulsar based navigation concept.

The first term on the right-hand side of Eq. (5) is the first order Doppler delay, and represents the simple geometric time delay between these two locations. The second term is due to the effects of parallax. Together these two terms are referred to as *Roemer* delay. The last term is the Sun's *Shapiro* delay effect, which is the additional time delay from the curved light ray path due to the Sun's gravity field[17]. If the relativistic effects are ignored, Eq. (6) reduces to the first order approximation as.

$$\Delta t = t_b - t_s = \boldsymbol{n} \cdot \boldsymbol{r}_b / c \tag{7}$$

C. Selection of Navigation Pulsar

Since the discovery of Scorpius X-1 in 1962, numerous experiments have been conducted to catalog the X-ray in the sky. These pulsars can be served as X-ray beacons for X-ray pulsar based navigation. Sala[20] selected ten rotation-powered X-ray pulsars from observations with ROSAT (short for Röntgensatellit, in German) and ASCA (Advanced Satellite for Cosmology and Astrophysics) missions, which can be used as candidate pulsars for navigation. The name, position, and period of these ten pulsars are listed in Table 1. In the table lo_E and la_E refer to Ecliptic longitude and latitude respectively.

Table 1 Characters of ten candidate X-ray pulsars

Name	lo_E (deg)	la_E (deg)	period (ms)
J0030+0451	8.91	1.45	4.8
B0633+17	98.11	-5.43	237.09
B1509-58	242.89	-39.40	150.23
B1929+10	297.05	32.29	226.51
J0437-47	50.47	-67.87	5.75
B1821-24	275.56	-1.55	3.05
B0656+14	104.64	-8.44	384.87
B0540-69	301.63	-86.66	50.37
J2124-33	312.74	-17.82	4.93
B1055-52	195.77	-52.39	197.10

At least three X-ray pulsars are needed for orbit determination. In order to select best three navigation pulsars from these candidates, Fisher information matrix is employed to optimize the unit direction of pulsars so that more information of spacecraft's state can be obtained from observations.

For simplicity, the measurements of X-ray pulsar based navigation can be modeled based on Eq. 6 and 7 as

$$y_i = \left[\boldsymbol{n}_i \cdot \left(\boldsymbol{r}_s - \boldsymbol{b}\right)\right] / c + \varepsilon_i = h_i(\boldsymbol{r}_s) + \varepsilon_i, \quad i = 1,2,3 \tag{8}$$

where ε_i is the measurement noise of the ith measurement, which is assumed as Gaussian white noise with the standard deviation of σ_i. Given three observations dependent on $\boldsymbol{r}_s$, the joint likelihood function is given by

$$L(y_1, y_2, y_3 \mid \boldsymbol{r}_s) = \prod_{i=1}^{3} \exp\left[-\left\| y_i - h_i(\boldsymbol{r}_s) \right\|^2 / (2\sigma_i^2) \right] / \sqrt{2\pi}\sigma_i \tag{9}$$

The maximum likelihood estimation of $\boldsymbol{r}_s$ is that which maximizes Eq. (9). This is equivalent to minimizing the negative log-likelihood function. Taking the negative of the natural log of Eq. (9) and retaining only terms dependent on $\boldsymbol{r}_s$, yields

$$J(\boldsymbol{r}_s) = \sum_{i=1}^{3} \left\| y_i - h_i(\boldsymbol{r}_s) \right\|^2 / (2\sigma_i^2) \tag{10}$$

The Fisher information matrix $\boldsymbol{F}$ is defined as the Hessian matrix of the $J(\boldsymbol{r}_s)$

$$\boldsymbol{F} = E\left\{ \frac{\partial^2}{\partial \boldsymbol{r}_s \partial \boldsymbol{r}_s^T} J(\boldsymbol{r}_s) \right\} = \sum_{i=1}^{3} \sigma_i^{-2} \frac{\partial h_i(\boldsymbol{r}_s)}{\partial \boldsymbol{r}_s} \left(\frac{\partial h_i(\boldsymbol{r}_s)}{\partial \boldsymbol{r}_s} \right)^T \tag{11}$$

Without loss of generality, standard deviations of ε_i are equal, thus

$$\sigma_i = \sigma, \quad i = 1, 2, 3 \tag{12}$$

The FIM can be reduced as

$$\boldsymbol{F} = \sigma^{-2} c^{-2} \sum_{i=1}^{3} \boldsymbol{n}_i \boldsymbol{n}_i^T \tag{13}$$

By means of the Cramér-Rao inequality[21], the estimated covariance can be bounded utilizing the Fisher information matrix

$$\boldsymbol{P} \geq \boldsymbol{F}^{-1} \tag{14}$$

where $\boldsymbol{P}$ is the error covariance of estimated $\boldsymbol{r}_s$. For navigation pulsar selection, the maximization of the determinant of FIM, which in fact is equivalent minimization of the condition number of FIM, is the objective. Additionally, because that

$$\det\left(\sum_{i=1}^{3} \boldsymbol{n}_i \boldsymbol{n}_i^T \right) = \left(\boldsymbol{n}_1 \cdot \left(\boldsymbol{n}_2 \times \boldsymbol{n}_3 \right) \right)^2 \tag{15}$$

the direction vectors of pulsars have to be chosen such that $(\boldsymbol{n}_1 \cdot (\boldsymbol{n}_2 \times \boldsymbol{n}_3))^2$ is maximum. Based on the candidates in Table 1, J0030+0451, B0633+17, and B0540-69 are selected as navigation pulsars, which are shown in Fig. 3.

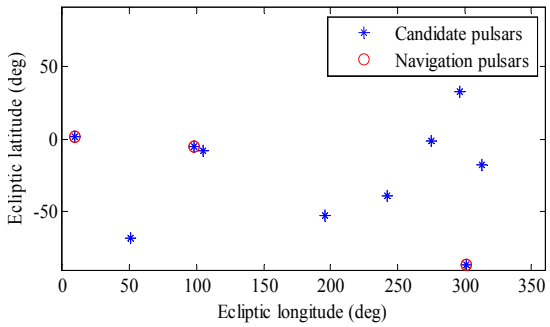

Figure 3. Navigation pulsars in ecliptic coordinate system.

III. Definition of Navigation Scenarios

The performance analysis used in the paper is based on the Curiosity spacecraft landing on Mars in August 2012. The approach phase started at 45 days before the spacecraft entered the Martian atmosphere. For the purpose of technology analysis, the final approach phase is defined as the period from 12 hours before atmospheric entry to the entry point at the Martian atmosphere. The entry point is defined at an altitude of 125 km above the Mars surface, and the entry conditions of Curiosity spacecraft in the Mars-centered inertial coordinate are listed in Table 2[12]. The Mars Reconnaissance Orbiter (MRO), which entered its Mars orbit in 2006, will function as the Mars Network orbiter in the analysis. The nominal orbital elements of the MRO mission are summarized in Table 3[12,22].

Table 2 Curiosity entry conditions

State vector element	Value
X , km	2509.459003
Y , km	377.697451
Z , km	-2442.509568
$\dot{X}$, km/s	-1.473129134
$\dot{Y}$, km/s	5.335713468
$\dot{Z}$, km/s	1.264687130

Table 3 Nominal orbital elements of the MRO

Orbital element	Value
Semimajor axis, km	3684.5
Eccentricity	0.010
Inclination, deg	93.0
Longitude of node, deg	278.0
Argument of periapsis, deg	270.0

In order to quantify the benefit of X-ray pulsar based navigation for Mars final approach, two navigation scenarios integrate with X-ray pulsar based navigation are initiated. In scenario 1, DSN navigation including Doppler, range, and ΔDOR measurements may be cut off until 6 hour before atmospheric entry because of severe time delay. However, with X-ray pulsar based navigation in the latter 6 hours of approach phase, the real-time navigation can still be established. In scenario 2, with Doppler and range measurement from MRO, Mars Network and X-ray pulsar based navigation are integrated together to compute the orbit determination in real time after the DSN tracking cut off. The timeline of two navigation scenarios in Mars final approach is illustrated in Fig. 4.

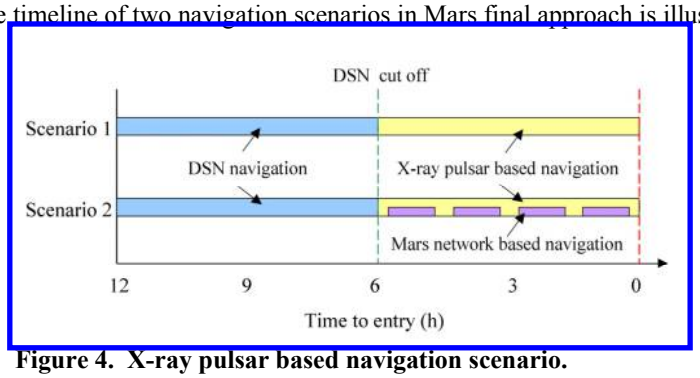

Figure 4. X-ray pulsar based navigation scenario.

However, the Mars Network based navigation can only be available when line-of-sight visibility exists between the spacecraft and MRO. To judge the visibility, two half angles are defined as

$$\theta_m = \arccos\left(R_M / |\boldsymbol{r}_m|\right), \quad \theta_s = \arccos\left(R_M / |\boldsymbol{r}_s|\right) \tag{16}$$

where R_M is the radius of Mars. Meanwhile, the angle between the Curiosity spacecraft and the MRO is given by

$$\theta = \arccos\left[\left(\boldsymbol{r}_m \cdot \boldsymbol{r}_s\right) / \left(|\boldsymbol{r}_m||\boldsymbol{r}_s|\right)\right] \tag{17}$$

Then the line-of-sight visibility the spacecraft and the MRO exist when following relationship is satisfied

$$\theta < \theta_m + \theta_s \tag{18}$$

The range and Doppler observations between the Curiosity spacecraft and the MRO are shown in Fig. 5

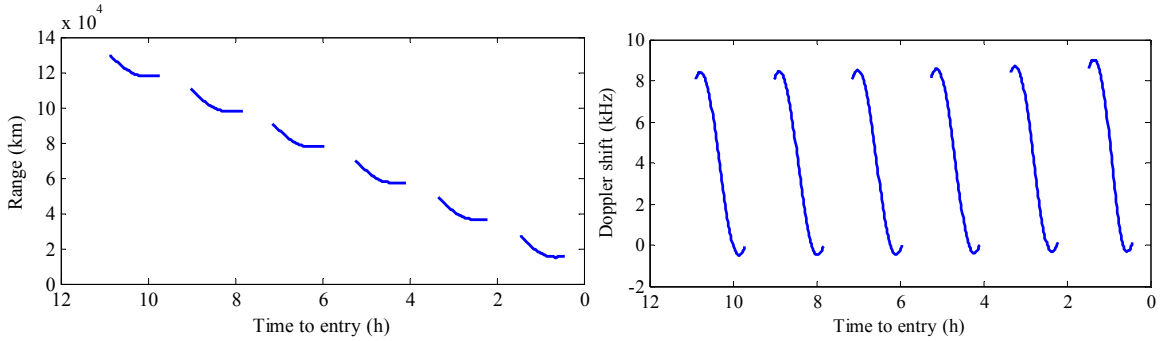

Figure 5. Range and Doppler observations between the Curiosity spacecraft and the MRO.

The blank portions of curve mean that Curiosity spacecraft can not be observed by MRO during the corresponding time. Thanks to the X-ray pulsar based navigation, real-time navigation in the final approach phase can still be achieved in these times.

IV. Navigation Filter Design

In the navigation filter, the 6 dimensional states vector for the Curiosity spacecraft consists of the position $\boldsymbol{r}_s$ and the velocity $\boldsymbol{v}_s$ in the heliocentric ecliptic coordinate system.

$$\boldsymbol{X} = \begin{bmatrix} \boldsymbol{r}_s \\ \boldsymbol{v}_s \end{bmatrix} \tag{19}$$

The dynamical model, which is used to propagate the spacecraft state and uncertainties, is governed by

$$\dot{\boldsymbol{X}} = \begin{bmatrix} \dot{\boldsymbol{r}}_s \\ \dot{\boldsymbol{v}}_s \end{bmatrix} = \begin{bmatrix} \boldsymbol{v}_s \\ -\mu_s \boldsymbol{r}_s / r_s^3 - \sum_{j=1}^{m} \mu_j \left(\boldsymbol{r}_{psj} / r_{psj}^3 - \boldsymbol{r}_{pj} / r_{pj}^3 \right) + \boldsymbol{a} \end{bmatrix} \tag{20}$$

where μ_s and μ_j are gravitational parameters of the Sun and the jth planet. $\boldsymbol{r}_{pj}$ refers to the position of the ith planet, and $\boldsymbol{r}_{psj}$ refers to the relative position of the spacecraft satisfying

$$\boldsymbol{r}_{psj} = \boldsymbol{r}_s - \boldsymbol{r}_{pj} \tag{21}$$

Furthermore, $\boldsymbol{a}$ indicates the unmodeled acceleration term.

Considering the nonlinear dynamical model and observation model, the ensemble square-root filter (EnSRF)[23,24] is utilized. In the first propagation step, a set of ensemble elements is generated using Monte Carlo sampling for the uncertain initial states, which initializes the assimilated elements. Then ensemble elements are propagated through nonlinear dynamical system independently, therefore the forecasted elements are obtained. Then the assimilated elements are optimally estimated in the assimilation step. The forecasted and assimilated elements can be written as

$$\begin{aligned} \boldsymbol{X}_k^f &= \bar{\boldsymbol{X}}^f + (\boldsymbol{X}_k^f)' \\ \boldsymbol{X}_k^a &= \bar{\boldsymbol{X}}^a + (\boldsymbol{X}_k^a)' \end{aligned}, \quad k = 1, \cdots, N \tag{22}$$

In the equation, $\bar{\boldsymbol{X}}^f$ and $\bar{\boldsymbol{X}}^a$ are the mean of forecasted and assimilated elements, and $(\boldsymbol{X}_k^f)'$ and $(\boldsymbol{X}_k^a)'$ denote the deviations from the mean. N refers to the size of ensemble elements for the initial state. $\bar{\boldsymbol{X}}^f$ and $(\boldsymbol{X}_k^f)'$ can be determined by propagated elements, and $\bar{\boldsymbol{X}}^a$ and $(\boldsymbol{X}_k^a)'$ are computed from the Kalman type data assimilation step, which is

$$\begin{aligned}\bar{\boldsymbol{X}}^a &= \bar{\boldsymbol{X}}^f + \boldsymbol{K}\left(\boldsymbol{y} - \boldsymbol{h}(\bar{\boldsymbol{X}}^f)\right)\\ (\boldsymbol{X}_k^a)' &= (\boldsymbol{X}_k^f)' - \tilde{\boldsymbol{K}}\boldsymbol{h}\left((\boldsymbol{X}_k^f)'\right)\end{aligned}, \quad k = 1, \cdots, N \tag{23}$$

where $\boldsymbol{h}$ denotes the nonlinear measurement operator, and $\boldsymbol{y}$ denotes the observation. Furthermore, the filter gain of $\boldsymbol{K}$ and $\tilde{\boldsymbol{K}}$ are defined by

$$\boldsymbol{K} = \boldsymbol{C}_{x^f h}(\boldsymbol{C}_h + \boldsymbol{C}_\varepsilon)^{-1} \tag{24}$$

$$\tilde{\boldsymbol{K}} = \boldsymbol{C}_{x^f h}\left(\left(\sqrt{\boldsymbol{C}_h + \boldsymbol{C}_\varepsilon}\right)^{-1}\right)^T \left(\sqrt{\boldsymbol{C}_h + \boldsymbol{C}_\varepsilon} + \sqrt{\boldsymbol{C}_\varepsilon}\right)^{-1} \tag{25}$$

where $\boldsymbol{C}_\varepsilon$ refers to the variance of measurement noise. Meanwhile, the variance of forecasted measurement $\boldsymbol{C}_h$ and covariance of forecasted state and measurement $\boldsymbol{C}_{x^f h}$ can be approximated by ensemble variance and covariance so that manipulation and storage of state covariance in EKF may be avoided.

V. Navigation Performance Analysis

In this section, a series of numerical simulations of the final approach are run to determine the navigation performance for two different navigation scenarios described in Section III. Furthermore, the accuracy analysis in the Mars B-plane is also conducted by evaluating the size of error ellipses generated by different navigation schemes.

The simulation starts at 24 hour before Mars entry, and the simulation results in the last 12 hours are focused. The initial triaxial position and velocity uncertainty (σ) is 5km and 10m/s, respectively. Without loss of generality, the measurement update rate of DSN tracking is one hour, while the measurement update rate of MRO tracking and X-pulsar observation is 5 minutes. The radial range and velocity measurement error of DSN tracking is 5 km and 1m/s (σ). MRO tracking data has an uncertainty of 100m and 0.1m/s (σ) in radial range and velocity measurements. Meanwhile, the X-pulsar observation gives range estimation of 3km (σ). The unmodeled accelerations in three axes are defined as zero mean Gaussian white noise with the deviation of 10^{-3}m/s^2. In the navigation filter, 20 ensemble elements are used for state and covariance propagation. The detailed simulation results are as follows.

A. DSN Tracking Combined with X-ray Pulsar based Navigation

The DSN measurement, which includes Doppler, range, and ΔDOR from DSN stations, is constantly provided until 6 hours before entry. During this period, the position and velocity of the Curiosity spacecraft can be accurately determined with reduced 3σ uncertainty bounds. However, if no observation is performed after the DSN tracking cut off, the state error may grow with the propagation due to the stochastic perturbations. Thanks to the X-ray pulsar based navigation implemented in the last 6 hours before entry, the real-time state estimation can still be computed. The navigation errors and 3σ uncertainty bounds of scenario 1 are illustrated in Fig. 6. After the DSN tracking cut off, the position and velocity error is further decreased because more accurate measurements are provided by X-ray pulsar observations. Meanwhile, the 3σ

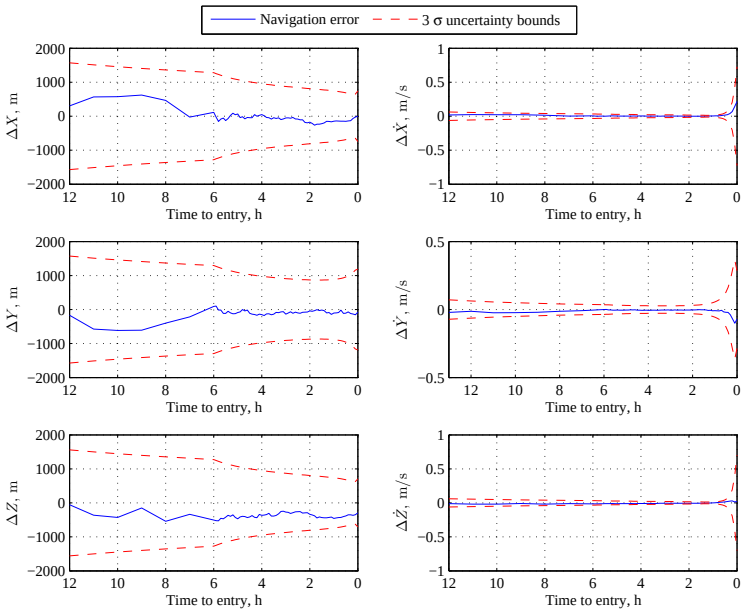

Figure 6. Estimation errors and 3σ uncertainty bounds for scenario 1.

uncertainty bound of position and velocity both decrease with time. Although the estimation errors diverge slightly which may caused by the relatively slow measurement update rate, large measurement error, and dramatic changes of states in the last half hours, position and velocity of spacecraft at entry point are still accurately estimated with 3σ uncertainties less than 1000m and 1m/s. Therefore, DSN tracking combined with X-ray pulsar based navigation can satisfy the requirement of navigation in final approach phase for future Mars landing missions.

B. DSN and MRO Tracking Combined with X-ray Pulsar based Navigation

In this navigation scenario, the navigation performance before DSN tracking cut off is the same as that for scenario 1. However, in the last 6 hours, the integrated navigation based on MRO tracking and X-ray pulsar observation can improve the accuracy and convergence of the real-time navigation system. Because the direction vector from the MRO to the Curiosity spacecraft is nearly aligned with the y axis, the position and velocity in this axis can be determined more accurately than those in x and z axis, which is shown in Fig. 7. In the invisible period, the Doppler and range measurements from MRO can not be provided, thus only X-ray pulsar measurements is available in this period. Nevertheless, the X-ray pulse based navigation can still hold the uncertainty bounds until the next visible period. Therefore the 3σ uncertainty bounds may fluctuate slightly. Furthermore, it can be concluded from Fig. 7 that the no obvious divergence of position error can be found in this scenario. The 3σ uncertainties of position and velocity in scenario 2 at the Mars entry point are about 500m and 0.5m/s. More accurate navigation results can be obtained with the implementation of MRO tracking data.

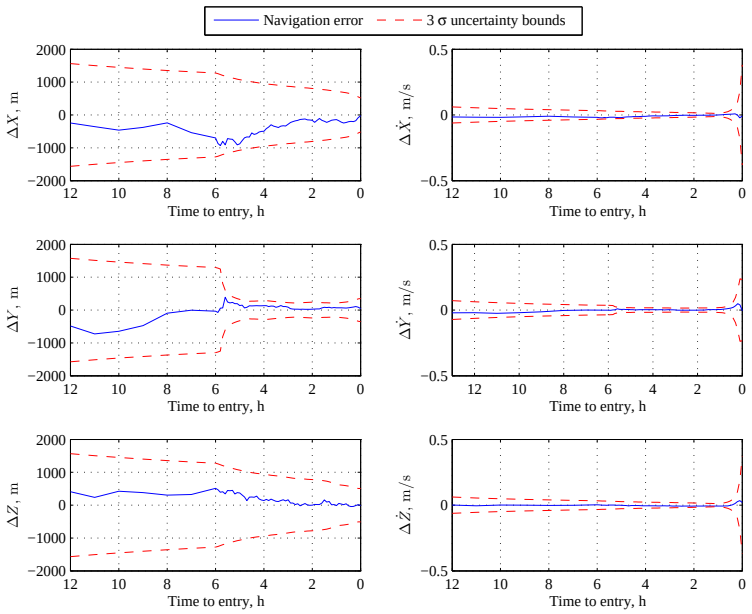

Figure 7. Estimation errors and 3σ uncertainty bounds for scenario 2.

C. Accuracy Analysis in Mars B-Plane

The targeting plane, which is commonly referred to as the B-Plane, is typically used for navigation and guidance to describe planetary approaching trajectories. Uncertainties in the approach trajectory can be mapped on the B-plane by error ellipses, so that more explicit conclusions may be drawn. A better estimation of approach trajectory is characterized by a smaller error ellipse in the B-plane.

To quantify the benefit of X-ray based navigation for Mars final approach, two more navigation scenarios are introduced. In scenario 3, DSN tracking is utilized as the only approach to navigation. After the tracking cut off, the state of the curiosity spacecraft is propagated through the dynamical model without any additional observations. Meanwhile in scenario 4, Doppler and range measurements from MRO is utilized after the DSN tracking cut off. However, in the invisible period, the state of spacecraft can only be propagated with dynamical model. For each navigation scenario, 1000 results are got from Monte-Carlo simulations. The error of estimated approach trajectory at entry point is represented on the Mars B-plane, and the accuracy analysis is performed on the B-plane by investigating the size of error ellipse. The 3σ error ellipses of different navigation scenarios are illustrated in Fig. 8.

The X-ray pulsar based navigation is a potential approach to improve the navigation performance in Mars final approach phase. The error ellipse of navigation based on DSN tracking and MRO tracking shrinks with the employment of X-ray based navigation. Although the position estimation in y axis of MRO tracking based navigation is more accurate, the orbit determination accuracy of MRO tracking based navigation and X-ray pulsar based navigation is almost the same. The 3σ error ellipsis of MRO tracking is only a little smaller than that of X-ray pulsar based navigation.

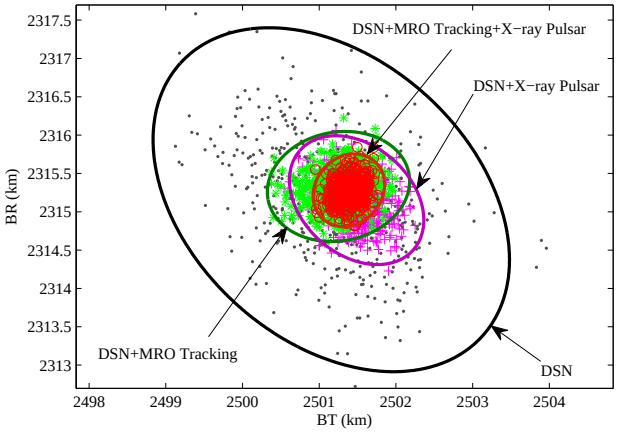

Figure 8. 3σ Error ellipses in Mars B-plane.

D. Distribution of Flight Path Angle

As an important parameter impacting on the accuracy of aerocapture and pinpoint landing, the accuracy of estimated flight path angle should be paid enough attention to. Although the normal flight path angle is -13.8002 deg, which is different from actual condition for Curiosity mission, it is still feasible to investigate the performance of navigation strategy. Again, we run Monte-Carlo simulation 1000 times, and the distributions of estimated FPA in 4 different scenarios are demonstrated in Fig, 9.

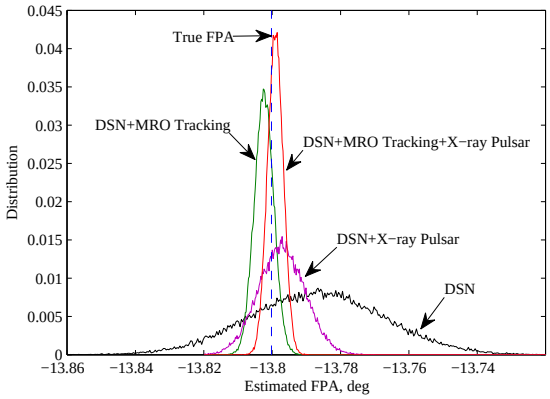

Figure 9. Distributions of estimated FPA.

It is shown that the navigation based on MRO tracking is the main contributor to improving the accuracy of FPA estimation. The X-ray pulsar based and MRO tracking based navigation has similar mean FPA, while the error bound of MRO tracking based navigation is much smaller. Therefore, the performance of velocity determination is improved with the implementation of MRO tracking data. Furthermore, with the help of X-ray pulsar based navigation, the bias and error bound of FPA are both decreased compared to scenario 3 and 4.

VI. Conclusion

This paper validates the feasibility of embedded X-ray pulsar based navigation to meet the technical need for real-time navigation in Mars final approach phase. Based on the 2012 encounter at Mars between the Curiosity spacecraft and the MRO spacecraft, two navigation scenarios combining with X-ray pulsar based navigation were considered, and the final approach of 12 hours before atmospheric entry was focused on. Simulations demonstrated that the X-ray pulsar based navigation could be integrated in the real-time navigation system for Mars final approach, and was capable of achieving 1000m and 1m/s or better 3σ uncertainty of position and velocity. Furthermore, two comparative navigation scenarios were introduced to quantify the benefits of X-ray pulsar based navigation by evaluating the error ellipse on the Mars B-plane. Finally, the distribution of flight path angle showed that the X-ray pulsar based navigation might improve the accuracy of state estimation at entry point. Therefore, X-ray pulsar based navigation is a potential navigation scheme for Mars final approach in the future.

Acknowledgments

This work was supported in part by the National Basic Research Program of China (973 Program) 2012CB720000, the National Natural Science Foundation of China 60874094, the Research Fund for the Doctoral Program of Higher Education of China 20111101110001, and the Science and Technology Innovation Team of Beijing Institute of Technology.

References

[1]NASA, "Solar System Exploration," Technical Report JPL 400-1077 5/03, May 2003.

[2]Way, D., Powell, R., Chen, A., and Steltzner, A., "Sensitivity Analysis of Design Parameters Affecting the Mars Science Laboratory Entry, Descent, and Landing System Altitude Performance and Timeline Margin," 2006 *IEEE Aerospace Conference*, IEEE Press, Piscataway, NJ, Mar. 2006. Paper 1465.

[3]Cangahuala, L. A., "Interplanetary Navigation Overview," *Proceedings of the 2000 IEEE/EIA International Frequency Control Symposium and Exhibition*, Kansas City, MO, Jun. 2000, pp. 618-621

[4]Martín-Mur, T. J., and Highsmith, D. E., "Mars Approach Navigation Using the VLBA", *21st International Symposium on Space Flight Dynamics*, Toulouse, France, Sep. 2009.

[5]Thornton, C. L., Border, J. S., "Radiometric Tracking Techniques for Deep-space Navigation," *Monograph 1, Deep Space Communications and Navigation Series*, Jet Propulsion Laboratory, California Institute of Technology, Pasadena, California.

[6]Magenta Books, "Delta-differential One Way Ranging (Delta-DOR) Operations," Recommended Practice, CCSDS 506.0-M-1, July, 2010.

[7]Bell, D. J., Cesarone, R., Ely, T. A.,Edwards, C., and Townes, S., "Mars Network: A Mars Orbiting Communications & Navigation Satellite Constellation," *IEEE Aerospace Conference IEEE Publications*, Piscataway, NJ, 18-25 Mar. 2000, pp. 75-88.

[8]Hastrup, R. C., Bell, D. J., Cesarone, R. J., Edwards, C. D., Ely, T. A., Guinn, J. R., Rosell, S. N., Srinivasan, J. M., and Townes, S. A., "Mars Network for Enabling Low-cost Missions," *Acta Astronautica*, Vol. 52, No. 2, Jan. 2003, pp. 227-235.

[9]Lévesque, J. F., and de Lafontaine, J., "Innovative Navigation Schemes for State and Parameter Estimation during Mars Entry," *Journal of Guidance Control and Dynamics*, Vol. 30, No. 1, 2007, pp. 169-184.

[10] Pastor, P. R., Gay, R. S., Striepe, S. A., Bishop, R., "Mars Entry Navigation from EKF Processing of Beacon Data," *HAIAA/AAS Astrodynamics Specialist Conference*, Denver, Colorado, Aug. 2000, AIAA 2000-4426.

[11] Ely, T. A., and Guinn, J. R., "Mars Approach Navigation Using Mars Network based Doppler Tracking," *Proceedings of the AIAA/AAS Astrodynamics Specialist Conference and Exhibit*, Monterey, California, Aug. 2002, AIAA 2002-4816.

[12] Lightsey, E.G., Mogensen, A.E., "Real-time Navigation for Mars Missions Using the Mars Network," *Journal of Spacecraft and Rockets*, Vol. 45, No. 3, 2008, pp. 519-533.

[13] Downs, G. S., "Interplanetary Navigation Using Pulsating Radio Sources," NASA Technical Reports N74-34150, 1974.

[14] Chester, T. J., and Butman, S. A., "Navigation Using X-ray Pulsars," NASA Technical Reports N81-27129, 1981.

[15] Graven, P., Collins, J., Sheikh, S., Hanson, J., Ray, P., and Wood, K., "XNAV for Deep Space Navigation," *31st Annual AAS Guidance and Control Conference*, Breckenridge, Colorado, Feb. 2008.

[16] Sheikh, S. I., Pines, D. J., Wood, K. S., Ray, P. S., Lovellette, M. N., and Wolff, M. T., "Spacecraft Navigation Using X-ray Pulsars," *Journal of Guidance, Control, and Dynamics*, Vol. 29, No. 1, 2006, pp. 49-63.

[17] Sheikh, S. I., "The Use of Variable Celestial X-ray Sources for Spacecraft Navigation," Ph.D. Dissertation, University of Maryland, College Park, Maryland, 2005.

[18] Emadzadeh, A. A., and Speyer, J. L., "Relative Navigation between Two Spacecraft Using X-ray Pulsars," *Control Systems Technology, IEEE Transactions on*, Vol. 19, No. 5, 2011, pp. 1021-1035.

[19] Graven, P. H., Collins, J. T., Sheikh, S. I., Hanson, J. E., "Spacecraft Navigation Using X-ray Pulsars," *7th International ESA Conference on Guidance, Navigation & Control Systems*, 2-5 Tralee, County Kerry, Ireland, Jun. 2008.

[20] Sala, J., Urruela, A., Villares, X., Estalella, R., and Paredes, J. M., "Feasibility Study for a Spacecraft Navigation System Relying on Pulsar Timing Information," European Space Agency Advanced Concepts Team ARIADNA Study 03/4202, Jun. 2004.

[21] Crassidis, J. L. and Junkins, J. L., *Optimal Estimation of Dynamic Systems, 2nd ed*., Boca Raton, Fl: Chapman & Hall/CRC, 2011.

[22] Jai, B., Wenkert, D., Halbrook, T., and Sidney, W., "The Mars Reconnaissance Orbiter Mission Operations: Architecture and Approach," *SpaceOps Conference*, Rome, Italy, Jun. 2006, AIAA 2006-5956.

[23] Tippett, M. K., Anderson, J. L., Bishop, C. H., Hamill, T. M., and Whitaker, J. S., "Ensemble Square Root Filters," *Mon. Weather Rev.*, Vol. 131, Jul. 2003,pp. 1485-1490.

[24] Li, J., Xiu, D., "On Numerical Properties of Ensemble Kalman Filter for Data Assimilation", *Comput. Methods Appl. Mech. Engrg*, Vol. 197, Apr. 2008, pp. 3574-3583.